Solution Structure of the Covalent Sterigmatocystin–DNA Adduct†

S. Gopalakrishnan,‡ Xiucai Liu,§ and Dinshaw J. Patel*,‡,∥

Department of Biochemistry and Molecular Biophysics, College of Physicians and Surgeons, Columbia University, New York, New York 10032, NMR Group, Sandoz Research Institute, East Hanover, New Jersey 07639, and Program in Cellular Biochemistry and Biophysics, Rockefeller Research Laboratories, Memorial Sloan-Kettering Cancer Center, New York, New York 10021

Received February 18, 1992; Revised Manuscript Received July 30, 1992

ABSTRACT: Sterigmatocystin and aflatoxin are potent mutagens that contaminate foodstuffs stored under conditions that permit fungal growth. These food mycotoxins can be metabolically activated to their epoxides, which subsequently form covalent adducts with DNA and can eventually induce tumor development. We have generated the sterigmatocystin–d(A1-A2-T3-G4-C5-A6-T7-T8) covalent adduct (two sterigmatocystins per duplex) by reacting sterigmatocystin-1,2-epoxide with the self-complementary d(A-A-T-G-C-A-T-T) duplex and determined its solution structure by the combined application of two-dimensional NMR experiments and molecular dynamics calculations. The self-complementary duplex retains its 2-fold symmetry following covalent adduct formation of sterigmatocystin at the N^7 position of G4 residues on each strand of the duplex. The H8 proton of [ST]G4 exchanges rapidly with water and resonates at 9.58 ppm due to the presence of the positive charge on the guanine ring following adduct formation. We have assigned the exchangeable and nonexchangeable proton resonances of sterigmatocystin and the duplex in the covalent adduct and identified the intermolecular proton–proton NOEs that define the orientation and mode of binding of the mutagen to duplex DNA. The analysis was aided by intermolecular NOEs between the sterigmatocystin protons with both the major groove and minor groove protons of the DNA. The molecular dynamics calculations were aided by 180 intramolecular nucleic acid constraints, 16 intramolecular sterigmatocystin constraints, and 56 intermolecular distance constraints between sterigmatocystin and the nucleic acid protons in the adduct. The sterigmatocystin chromophore intercalates between the [ST]G4·C5 and T3·A6 base pairs and stacks predominantly over the modified guanine ring in the adduct duplex. The overall conformation of the DNA remains right-handed on adduct formation with unwinding of the helix, as well as widening of the minor groove. Parallel NMR studies on the sterigmatocystin–d(A1-A2-A3-G4-C5-T6-T7-T8) covalent adduct (two sterigmatocystins per duplex) provide supportive evidence that the mutagen covalently adducts the N^7 position of G4 and its chromophore intercalates to the 5′ side of the guanine and stacks over it. The present NMR–molecular dynamics studies that define a detailed structure for the sterigmatocystin–DNA adduct support key structural conclusions proposed previously on the basis of a qualitative analysis of NMR parameters for the adduct formed by the related food mutagen aflatoxin B_1 and DNA [Gopalakrishnan, S., Harris, T. M., & Stone, M. P. (1990) *Biochemistry 29*, 10438–10448].

Sterigmatocystin is a mycotoxin produced by some strains of *Aspergillus*, *Penicillium*, and *Bipolaris sp.* (Holzapfel et al., 1966; Schroeder & Kelton., 1975). It is a precursor of aflatoxins B_1, B_2, G_1, and G_2 (Dutton, 1988; Yabe et al., 1988, 1989; Bhatnagar et al., 1989, 1991). Sterigmatocystin occurs in various foodstuffs susceptible to fungal growth along with aflatoxins albeit in lesser quantities [reviewed in Busby and Wogan (1984)]. Sterigmatocystin is hepatotoxic to laboratory animals. The target organs include lung, stomach, kidney, and duodenum. (Purchase & Van der Watt, 1969; Van der Watt & Purchase, 1970; Wang et al., 1991; Sreemannarayana et al., 1989). Several animal model studies have suggested that sterigmatocystin is primarily a hepatocarcinogen but also produces squamous cell carcinoma, adenocarcinoma of the lung, and bone tumors (Xie, 1990; Adamson, 1989; Mori et al., 1988; Dickens et al., 1966; Purchase & Van der Watt, 1970, 1973). In vitro studies have established that sterigmatocystin is mutagenic (Krivobok et al., 1987). The carcinogenicity as well as the mutagenicity of sterigmatocystin is approximately 10-fold lower than that of aflatoxin B_1. In the umu assay, sterigmatocystin showed higher response than aflatoxin B_1 (Baertschi et al., 1989). Several epidemiological studies have suggested that aflatoxins might be involved in human liver cancers [reviewed in Busby and Wogan (1984); see also Stoloff (1989) for an opposing view]. Recent studies on mutations of the p53 tumor suppressor gene in human subjects suggested that aflatoxins might be linked to the G to T transversions at codon 249 (Bressac et al., 1991; Hsu et al., 1991).

Sterigmatocystin **1** is structurally similar to aflatoxin B_1 **2**. It is activated by liver microsomes to form a N^7-guanine adduct similar to aflatoxin B_1 (Essigmann et al., 1977, 1979; Croy et al., 1978). The carcinogenicity, as well as the toxicity, requires the presence of the double bond at the 1,2 position and the activated species is presumed to be the 1,2-epoxide of sterigmatocystin **3**. Various studies postulated an intermediate cationic adduct at the N^7 of guanine to be the primary adduct with DNA. The epoxide has not been isolated by enzymatic activation. However, the laboratory of T. M. Harris has successfully chemically synthesized the epoxide of aflatoxin B_1 and showed that it can bind DNA without metabolic activation to form the N^7-guanine adduct previously identified from biological systems (Baertschi et al., 1988). The postulated N^7-guanine cationic adduct of aflatoxin B_1 was also

† This research was funded by Columbia University Start-Up funds and NIH Grant CA46533.

* To whom correspondence should be addressed.
‡ Columbia University.
§ Sandoz Research Institute.
∥ Memorial Sloan-Kettering Cancer Center.

0006-2960/92/0431-10790$03.00/0

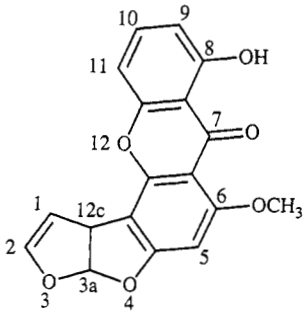

STERIGMATOCYSTIN

1

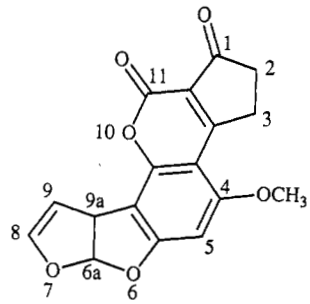

AFLATOXIN B1

2

verified by the same research group following characterization of the adduct at the oligodeoxynucleotide level (Gopalakrishnan et al., 1989). The adduct formation was shown to exhibit a stoichiometry of one aflatoxin B_1 per duplex in the case of d(A-T-C-G-A-T) while the isomeric sequence d(A-T-G-C-A-T) bound two aflatoxin B_1 molecules per duplex (Gopalakrishnan et al., 1990). Using high-field NMR spectroscopy, it was established that aflatoxin B_1 intercalated into the duplex on the 5′ side of the adducted guanine (Gopalakrishnan et al., 1990).

Though sterigmatocystin metabolism is similar to aflatoxin B_1, it has not been studied in sufficient detail. Our interest stems from the fact that sterigmatocystin and aflatoxin B_1 contain the same reactive functionality, but sterigmatocystin elicits reduced mutagenic and carcinogenic response. Herein we describe our studies on elucidating the three-dimensional solution structure of the cationic sterigmatocystin–DNA adduct at the N^7 of guanine **4**. The previous studies on

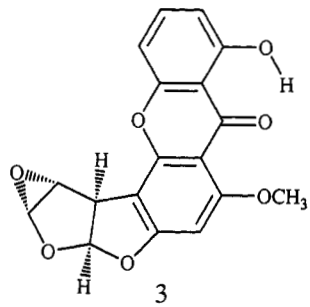

3

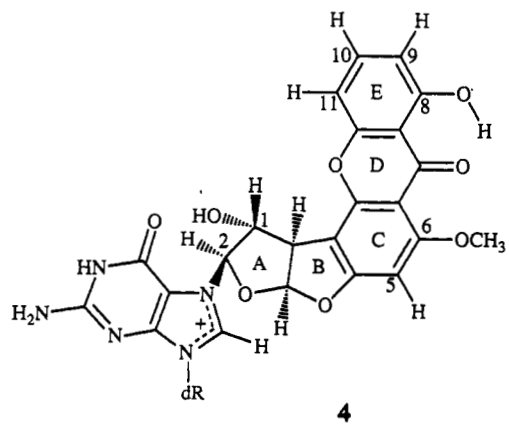

4

aflatoxin B_1 (Gopalakrishnan et al., 1990) reported on qualitative structural features of the aflatoxin B_1–DNA adduct while the present study extends these observations to a quantitative three-dimensional solution structure of the sterigmatocystin–DNA adduct based on a combined application of NMR and restrained molecular dynamics calculations.

The dangers of the aflatoxin family of mycotoxins to human health was recently reinforced by the demonstration that guanine alkylation by aflatoxin represents the source of G to A base substitutions in the p53 tumor suppressor genes in humans (Hsu et al., 1991; Bressac et al., 1991). Similar reports of base substitution mutations have also been reported for bulky intercalating mutagens which react with the N^7 of guanine (Sahasrabudhe et al., 1989, 1990). The structure of the primary N^7-guanine adduct, as well as its degradation products, will be of primary importance in efforts to correlate structure–activity–function relationships within this family of mycotoxins.

MATERIALS AND METHODS

Synthesis of Oligodeoxynucleotides. Oligodeoxynucleotides were synthesized on an Applied Biosystems automated synthesizer using cyanoethylphosphoramidites. All reagents for the oligodeoxynucleotide synthesis were purchased from Applied Biosystems. The resulting dimethoxytrityl protected oligonucleotide was purified in two steps on a C4-HPLC column and desalted using G-25 Sephadex gel. The counterion was exchanged with sodium using an ion-exchange column.

Synthesis of Sterigmatocystin–Oligonucleotide Adducts. Sterigmatocystin was purchased from Sigma. Dimethyldioxirane was prepared as a 0.05 M solution in acetone (Murray & Jayaraman, 1985). Sterigmatocystin was dissolved in methylene chloride and reacted with 2-fold excess of dimethyldioxirane, resulting in quantitative conversion to sterigmatocystin-1,2-epoxide (Baertschi et al., 1988).

Purified octamers d(A-A-T-G-C-A-T-T) and d(A-A-A-G-C-T-T-T) were prepared as mentioned above and dissolved in 1 mL of aqueous buffer (0.01 M sodium phosphate, 0.1 M NaCl, pH 7.0). Sterigmatocystin-1,2-epoxide is not soluble in water. Roughly 5 mg of the epoxide present in 1 mL of methylene chloride was added to approximately 300 A_{260} units of the deoxyoctanucleotide. The reactants were stirred at 5 °C in a polypropylene tube. The reaction was monitored over a period of 7 days using analytical C18-HPLC. Generally, the reaction proceeds to about 40–50% modification in 7 days, at which stage the reaction is stopped. The aqueous layer is partitioned three times with fresh methylene chloride to remove unbound sterigmatocystin byproducts and purified on a C4 preparative HPLC column. The loading buffer was 0.01 M sodium phosphate (pH 6.9), and the eluant was acetonitrile. The elution profiles were similar to those of aflatoxin–oligonucleotide adducts (Gopalakrishnan et al., 1989). The isolated adduct exhibited broad UV maxima around 310 nm characteristic of the sterigmatocystin chromophore. The sterigmatocystin–oligonucleotide adduct was then desalted using Sephadex G-25, and the counterion was exchanged with sodium using Dowex 50X8 cation-exchange column.

For NMR experiments, all samples were dissolved in 0.4 mL of aqueous buffer (0.01 M sodium phosphate, 0.1 M sodium chloride, 0.001 M EDTA, pH 7.0) and lyophilized. For experiments in H_2O, the samples were redissolved in 90% H_2O/10% D_2O. For experiments in D_2O, the samples were relyophilized three times in 99.8% D_2O and finally dissolved in 0.4 mL of 99.96% D_2O. All samples were degassed for 10 min. The adduct is unstable and depurinates easily at room temperature. Hence the samples were kept in the freezer between experiments to avoid depurination. All NMR experiments were performed at 5 °C.

NMR Experiments. All NMR spectra were recorded on Bruker AM 500 or AM 400 spectrometers. Quadrature detection was used in both dimensions with the carrier

frequency placed on the H_2O resonance for all experiments. All data sets were transferred to a VAX 11-780 or a micro VAX II computer and processed with the FTNMR program (Hare Research). The FIDs for the initial t_1 value in each two-dimensional data set were multiplied by 0.5 in order to eliminate t_1 ridge artifacts.

Two-dimensional NOESY data sets of the d(A1-A2-T3-[ST]G4-C5-A6-T7-T8) and d(A1-A2-A3-[ST]G4-C5-T6-T7-T8) duplexes were recorded in D_2O at 5 ± 0.5 °C on a Bruker AM 500 spectrometer. The spectral width was 9 ppm. Continuous low-power irradiation of the residual water signal was applied during the recycle time for all spectra in D_2O. A HOHAHA spectrum was recorded in the adduct d(A1-A2-T3-[ST]G4-C5-A6-T7-T8) with a spin lock time of 80 ms in D_2O solution.

The NOESY specta of the adducts were recorded in H_2O with 2048 complex points in t_2, 512 complex points in t_1, and 160 scans for each FID. The sample temperature was 5 ± 0.5 °C, and the spectral width was 20 ppm. The water signal was suppressed by a jump and return pulse sequence as the detection pulse (Plateau & Gueron, 1982). The relaxation time was 1.2 s, and the mixing time was 150 ms. The delay time between the pulses was set to 60 μs to optimize the excitation in imino, amino, and aromatic proton regions of the adduct.

Interproton Distance Constraints. For distance measurements in the d(A1-A2-T3-[ST]G4-C5-A6-T7-T8) adduct duplex, sets of NOESY spectra were collected at 50- and 75-ms mixing times at 5 °C with 2048 complex points in t_2, 128 transients for each FID, and a repetition delay of 2.0 s. Both time-domain data sets were multipled by a 90° phase-shifted sine bell window function. The initial slopes were computed and approximate distances estimated using the two-spin approximation and calibration against buildups for fixed interproton distances. The interproton distances involving base–base, base–sugar H3′, base–sugar H1′, and sterigmatocystin nonexchangeable protons were calculated using the cytidine H5–H6 distance of 2.5 Å as a reference, those involving methyl groups were calculated using the thymidine H6–CH_3 distance of 2.9 Å as a refrence, and those involving other nonexchangeable protons were calculated using the sugar H2′–H2″ distance of 1.8 Å. Distance bounds were generally set at ±30%. For exchangeable protons, the distances were roughly estimated from the relative strength of the cross peaks in the NOESY spectrum in H_2O recorded at a mixing time of 150 ms. Strong cross peaks were given a bound of 2.0–4.0 Å and medium cross peaks a bound of 2.5–5.0 Å. Weak cross peaks were not utilized for distance measurements.

Structure Computations. The initials models of the d(A1-A2-T3-[ST]G4-C5-A6-T7-T8) adduct were generated using QUANTA (Polygen Corporation). All energy minimization and molecular dynamics calculations were carried out on a Convex C2 computer using the XPLOR program (A. Brunger, Yale University). The general procedures for the energy minimization and molecular dynamics calculations have been described previously (Zhang & Patel, 1990, 1991). Two different starting models were generated for the adduct and the refinement guided by the input distance constraints available from NMR analysis. Each starting structure was first subjected to 500 cycles of energy minimization in order to relieve bad contacts between nonbonded atoms. During this energy minimization, the hydrogen-bond constraints for DNA base pairs were used to retain Watson–Crick pairing in the DNA duplex. The structure was then subjected to molecular dynamics refinement in two stages, namely, the high-temperature stage and the cooling/equilibration stage using protocols similar to those described elsewhere (Zhang & Patel, 1990, 1991). In general, 8 ps of high-temperature dynamics and 8 ps of dynamics at the cooling/equilibration stage were performed.

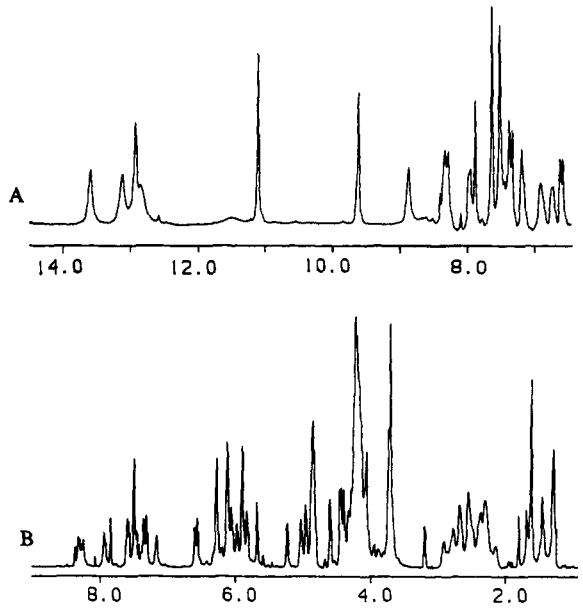

FIGURE 1: Proton NMR spectra of the d(A-A-T-[ST]G-C-A-T-T) adduct duplex in aqueous buffer (100 mM NaCl, 10 mM phosphate, 1 mM EDTA), pH 7.0, at 5 °C. (A) Exchangeable proton spectrum (6.5–14.0 ppm) in H_2O solution. (B) Nonexchangeable proton spectrum (1.0–8.5 ppm) in D_2O solution.

RESULTS

Stoichiometry of the Adduct. Sterigmatocystin-1,2-epoxide is poorly soluble in water. Hence it was dissolved in methylene chloride and reacted with DNA oligomer in aqueous buffer. The slow reaction was monitored by C18 reverse-phase analytical HPLC. The optimum condition for the reaction was about 7 days, at which stage the modification was about 40–50% complete. The C18 reverse-phase HPLC analysis of the crude reaction mixture suggested that the depurination and hydrolysis products of the adduct increase over time. It was clear that the reaction stoichiometry was two sterigmatocystins per d(A-A-T-G-C-A-T-T) duplex and d(A-A-A-G-C-T-T-T) duplex. The pure adduct was collected as a single peak eluting from the C4 preparative HPLC column having characteristic absorbances at 260 and 310 nm. NMR spectra of the adducts were taken to identify the presence of sterigmatocystin chromophore and to define the nature of the adduct duplex. The proton NMR spectra of the d(A1-A2-T3-[ST]G4-C5-A6-T7-T8) adduct duplex **5** in H_2O and D_2O at 5 °C are shown in Figure 1, panels A and B, respectively.

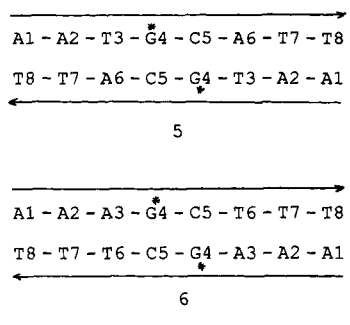

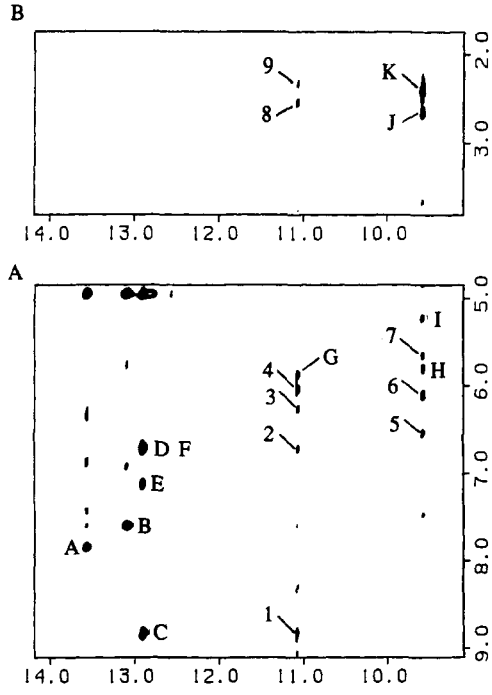

FIGURE 2: Expanded NOESY contour plots (mixing time, 150 ms) of the d(A-A-T-[ST]G-C-A-T-T) adduct duplex in H_2O buffer at 5 °C. (A) Contour plot correlating the 9.0–14.0 ppm region with the 5.0–9.0 ppm region. (B) Contour plot correlating the 9.0–14.0 ppm region with the 2.0–4.0 ppm region. The NOE cross peaks A–K are assigned as follows: (A) T7(NH1)–A2(H2); (B) T3(NH1)–A6(H2); (C) [ST]G4(NH1)–[ST]G4(NH_2-b); (D) [ST]G4(NH1)–[ST]G4(NH_2-e); (E) [ST]G4(NH1)–C5(NH_2-b); (F) [ST]G4-(NH1)–C5(NH_2-e), (G) ST(OH-8)–ST(H9); (H) [ST]G4(H8)–[ST]G4(H1′); (I) [ST]G4(H8)–C5(H5); J [ST]G4(H8)–[ST]-G4(H2″); (K) [ST]G4(H8)–[ST]G4(H2′). The intermolecular NOE cross peaks 1–9 are assigned as follows: (1) ST(OH-8)–[ST]-G4(NH_2-b); (2) ST(OH-8)–[ST]G4(NH_2-e); (3) ST(OH-8)–A6-(H1′); (4) ST(OH-8)–C5(H1′); (5) [ST]G4(H8)–ST(H3a); (6) [ST]G4(H8)–ST(H2); (7) [ST]G4(H8)–ST(H5); (8) ST(OH-8)–C5(H2″); (9) ST(OH-8)–C5(H2′).

The spectrum recorded in H_2O clearly establishes the presence of four hydrogen-bonded imino protons (12.6–13.8 ppm) in the d(A-A-T-[ST]G-C-A-T-T) adduct duplex (Figure 1A). The spectrum recorded in D_2O shows signals in the aromatic region arising from sterigmatocystin protons (Figure 1B). The lines are sharp, indicative of a single conformation for the d(A-A-T-[ST]G-C-A-T-T) adduct duplex in aqueous solution. A narrow and slowly exchanging peak appears around 9.58 ppm in the spectrum recorded in H_2O (Figure 1A). Such a peak has been previously observed for G(H8) proton in an aflatoxin B_1–N^7-guanine cationic adduct at the DNA oligomer duplex level (Gopalakrishnan et al., 1989, 1990). We also detect minor resonances in the proton spectra of the d(A-A-T-[ST]G-C-A-T-T) adduct duplex in aqueous solution (Figure 1), and these are assigned to components resulting from adduct degradation since they increase with time.

Exchangeable Proton Assignments. The spectrum of d(A-A-T-[ST]G-C-A-T-T) adduct duplex in H_2O at 5 °C exhibits six exchangeable proton resonances in the 9.0–14.0 ppm region (Figure 1A). Four of the resonances occur in the hydrogen-bonded imino proton region of the spectrum while two sharp peaks are observed at 11.06 and 9.58 ppm. The imino resonances occurring at 13.56 and 13.09 ppm exhibit NOE cross peaks to the A2(H2) (peak A, Figure 2) and the A6-(H2) (peak B, Figure 2) protons, respectively, and are therefore assigned to the T7(NH3) and T3(NH3) protons, respectively. [The assignments of A(H2) protons are presented in a later section.] The T8(NH3) imino proton is broadened by exchange and does not show an NOE in the NOESY spectrum of the adduct. The remaining imino proton at 12.89 ppm was assigned to the G4(NH1) proton on the basis of the observed NOEs to the G4(NH_2-2) (peaks C and D, Figure 2) and C5(NH_2-4) (peaks E and F, Figure 2) amino protons. Interestingly, we observe separate resonances for the hydrogen-bonded and exposed G4(NH_2-2) protons in the adduct.

Table I: Chemical Shifts of Exchangeable Nucleic Acid Protons in the d(A-A-T-[ST]G-C-A-T-T) Adduct Duplex in H_2O Buffer at 5 °C

	chemical shifts (ppm)			
residue	NH1	NH3	NH_2-2	NH_2-4
T3		13.09		
[ST]G4	12.89		8.83, 6.71	
C5				7.12, 6.71
T7		13.56		
T8		12.89		

The resonance at 9.58 ppm can be assigned to H8 proton of [ST]G4 on the basis of its NOEs to the H1′ (peak, H, Figure 2), H2′ (peak K, Figure 2), H2″ (peak J, Figure 2), and H3′ proton of [ST]G4 and the H5 proton of C5 (peak I, Figure 2). The resonance at 11.06 ppm is assigned to the OH-8 proton of sterigmatocystin on the basis of an NOE observed to the H9 proton of sterigmatocystin (peak G, Figure 2). The exchangeable nucleic acid proton assignments for the d(A-A-T-[ST]G-C-A-T-T) adduct duplex at 5 °C are listed in Table I.

Nonexchangeable Nucleic Acid Proton Assignments. The nonexchangeable nucleic acid proton assignments in right-handed DNA can be monitored by tracing the sequential NOE connectivities between the base protons and their own and 5′-linked sugar protons (Wüthrich, 1986). Such tracings for the d(A1-A2-T3-[ST]G4-C5-A6-T7-T8) adduct duplex from the base (purine H8 and pyrimidine H6) protons to the sugar H1′ protons are plotted in Figure 3A and to the sugar H3′ protons are plotted in Figure 3B. There is a break in the connectivity between the H8 proton of A6 and the sugar H1′ (see arrow, Figure 3A) and sugar H3′ (see arrow, Figure 3B) protons of C5 at the C5–A6 step for the adduct duplex. The H8 proton of [ST]G4 at 9.58 ppm exchanges out rapidly in D_2O solution and hence can only be observed in the adduct duplex in H_2O solution. We detect an NOE between the H8 proton of [ST]G4 and its own H1′ proton (peak H, Figure 2) but not to the H1′ proton of T3, establishing a break in the connectivity at the T3–[ST]G4 step in the adduct duplex. These breaks in the distance connectivities for the T3–ST-[G4] and C5–A6 steps in the d(A1-A2-T3-[ST]G4-C5-A6-T7-T8) adduct duplex are confirmed by monitoring the NOE patterns in the expanded NOESY plot of the base to sugar H2′,2″ proton region (Figure 4).

The observation of base (purine H8 or pyrimidine H6) to base (pyrimidine H5 or CH_3-5) NOEs for the A2–T3 (peak B, Figure 4), [ST]G4–C5 (peak I, Figure 2), A6–T7 (peak A, Figure 4), and T7–T8 (peak C, Figure 4) steps establishes normal base stacking with a right-handed directionality at these steps in the adduct.

The H2 protons of A1, A2, and A6 were differentiated on the basis of NOEs to their own assigned sugar H1′ protons in the adduct duplex. Further, the resolved A2(H2) proton at 7.80 ppm exhibits NOEs to the partially resolved A1(H2) and A6(H2) protons between 7.53 and 7.57 ppm. The nonexchangeable nucleic acid proton assignments for the adduct duplex at 5 °C are listed in Table II.

Nonexchangeable Sterigmatocystin Proton Assignments. The nonexchangeable protons of the sterigmatocystin moiety

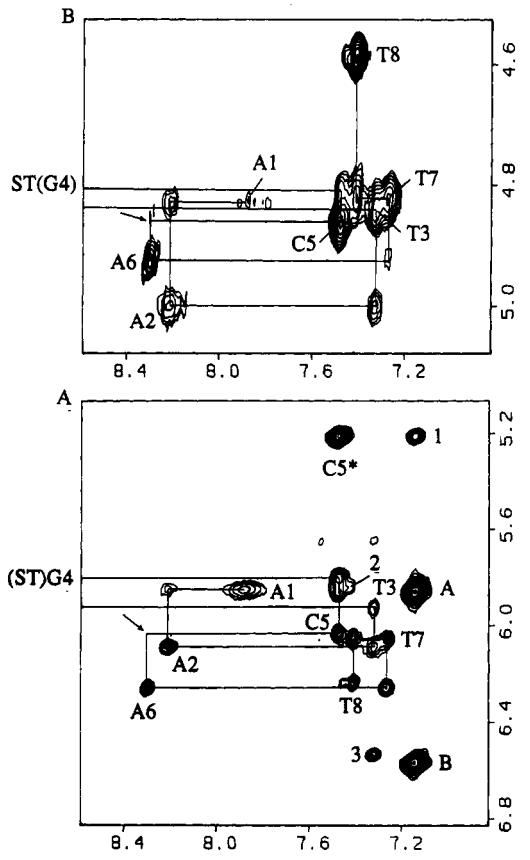

FIGURE 3: Expanded NOESY contour plots (mixing time, 75 ms) of the d(A-A-T-[ST]G-C-A-T-T) adduct duplex in D_2O buffer at 5 °C. (A) Contour plot correlating the base protons (6.8–8.4 ppm) with the sugar H1′ and cytidine H5 protons (5.1–6.8 ppm). (B) Contour plot correlating the base protons (6.8–8.4 ppm) with the sugar H3′ protons (4.5–5.1 ppm). The lines trace the connectivities between the base and their own and 5′-flanking sugar protons. C5* represents the NOE between C5(H5) and C5(H6). Intramolecular sterigmatocysin cross peaks A and B are assigned as follows: (A) ST(H10)–ST(H9); (B) ST(H10)–ST(H11). Intermolecular cross peaks 1–3 are assigned as follows: (1) ST(H10)–C5(H5); (2) ST-(H9)–C5(H6); (3) ST(H3a)–T3(H6).

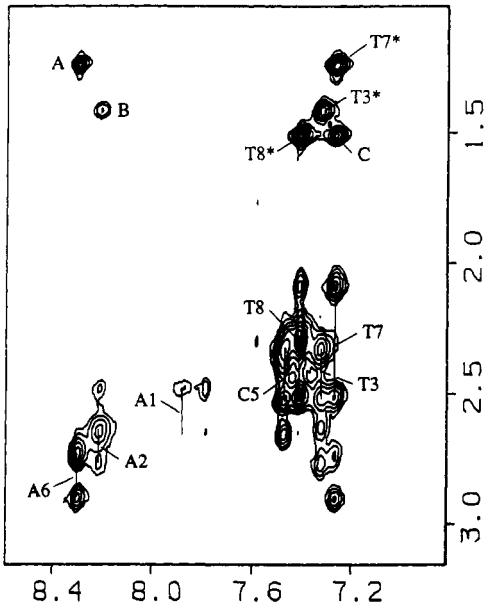

FIGURE 4: Expanded NOESY contour plot (mixing time, 75 ms) of the d(A-A-T-[ST]G-C-A-T-T) adduct duplex in D_2O buffer at 5 °C. The contour plot correlates the base protons (7.0–8.4 ppm) with the H2′, H2″, and thymine methyl protons (1.0–3.0 ppm). The labeled cross peaks correspond to NOEs between the base protons and their own sugar H2′,2″ protons. NOEs between H6 and CH_3 protons within individual thymines are labeled T3*, T7*, and T8*. Cross peaks A–C are assigned as follows: (A) A6(H8)–T7(CH_3); (B) A2-(H8)–T3(CH_3); (C) T7(H6)–T8(CH_3).

can be assigned by following the through-space and through-bond connectivity patterns. The 7.13 ppm aromatic proton exhibits strong NOE cross peaks to protons at 6.55 (peak B, Figure 3) and 5.84 ppm (peak A, Figure 3), with the latter two exhibiting a weaker NOE among themselves. This kind of NOE pattern can be identified with the aromatic H9, H10, and H11 ring protons. Proton H10 exhibits strong coupling cross peaks to H9 and H11 in the COSY spectrum as well. We can identify a cross peak from the OH-8 proton to the proton at 5.84 ppm (peak G, Figure 2) but not to the proton at 6.55 ppm, thus differentiating between the H9 and H11 protons. Protons of the bisdihydrofuran moiety can also be assigned in a similar manner. Protons H3a and H12c are cis to each other and exhibit a strong coupling, as well as an NOE cross peak. By contrast, protons H1 and H2 exhibit a very weak coupling cross peak, and this observation has implications for the stereochemistry of these five-membered ring protons in the covalent adduct. Further, proton H3a exhibits a stronger NOE cross peak to the H2 proton (peak A, Figure 5) because it lies on the same side as H3a and exhibits a weaker NOE cross peak to the H1 proton (peak C, Figure 5), which lies on the opposite side of H3a. Additional support for the assignment of H2 can be provided from an intermolecular NOE observed between the sterigmatocystin H2 proton and the [ST]G4(H8) proton (peak 6, Figure 2) at the covalent linkage site. The OCH_3-6 and H5 protons do not exhibit coupling connectivities to any other protons but exhibit an NOE cross peak between themselves (peak F, Figure 5). Thus, the OCH_3-6 and H5 protons can be identified at 3.66 and 5.63 ppm, respectively, in the adduct duplex spectrum. The sterigmatocystin proton assignments for the adduct duplex at 5 °C are listed in Table III.

Intermolecular NOE Contacts between Sterigmatocystin and DNA. We detect a number of intermolecular NOEs between the sterigmatocystin and the DNA protons in the NOESY spectrum of the d(A-A-T-[ST]G-C-A-T-T) adduct duplex. The sterigmatocystin protons can be subdivided into those on the bisdihydrofuran moiety (H1, H2, H3a, and H12c), the aromatic ring carrying the methoxy group (H5 and OCH_3-6) and the phenolic ring (OH-8, H9, H10 and H11). The ST(H2) proton at the covalent linkage site exhibits NOEs to the major groove [ST]G4(H8) proton (peak 6, Figure 2A) and the C5(H5) proton (peak 1, Figure 5). This implies that the ST(H2) proton is positioned in the major groove and directed toward the [ST]G4–C5 step. The ST(H3a) proton exhibits NOEs to the major groove T3(H6) (peak 3, Figure 3A) and T3(CH_3) (peak 13, Figure 5) protons, as does the ST(H12c) proton to the same major groove protons. This positions the bridgehead ST(H3a) and ST(H12c) protons on the bishydrofuran ring in the major groove and directed toward T3 in the T3–[ST]G4 step.

The ST(H5) aromatic proton exhibits NOEs to the minor groove A6(H2), [ST]G4(H1′) (peak 3, Figure 5), and T3-(H1′) (peak 2, Figure 5) protons, as does the ST(OCH_3-6) aromatic protons to the same minor groove protons. These observations position the sterigmatocystin aromatic ring edge containing the H5 and OCH_3-6 protons in the minor groove between the [ST]G4·C5 and the A2·T7 base pairs.

The ST(OH-8) aromatic ring proton exhibits NOEs to the minor groove [ST]G4 (NH_2-2b) (peak 1, Figure 2), [ST]-G4(NH_2-2e) (peak 2, Figure 2), A6(H1′) (peak 3, Figure 2), and C5(H1′) (peak 4, Figure 2) protons establishing that the

Table II: Chemical Shifts of Nonexchangeable Protons in the d(A-A-T-[ST]G-C-A-T-T) Adduct Duplex in D_2O Buffer at 5 °C

	chemical shifts (ppm)								
residue	H8/H6	H5/CH_3	H2	H1′	H2′	H2″	H3′	H4′	H5′, H5″
A1	7.88		7.57	5.84	2.49	2.66	4.82	4.21	3.70
A2	8.21		7.80	6.07	2.66	2.70	4.99	4.40	4.18
T3	7.32	1.42		5.91	2.34	2.52	4.83	4.20	
[ST]G4	9.58[a]			5.78	2.39	2.66	4.79	4.37	4.19
C5	7.47	5.20		6.01	2.34	2.53	4.85	4.18	
A6	8.30		7.53	6.24	2.75	2.91	4.91	4.44	4.29
T7	7.27	1.25		6.04	2.09	2.52	4.81	4.22	
T8	7.41	1.52		6.21	2.29	2.29	4.58	4.02	4.20

[a] Chemical shift in H_2O solution.

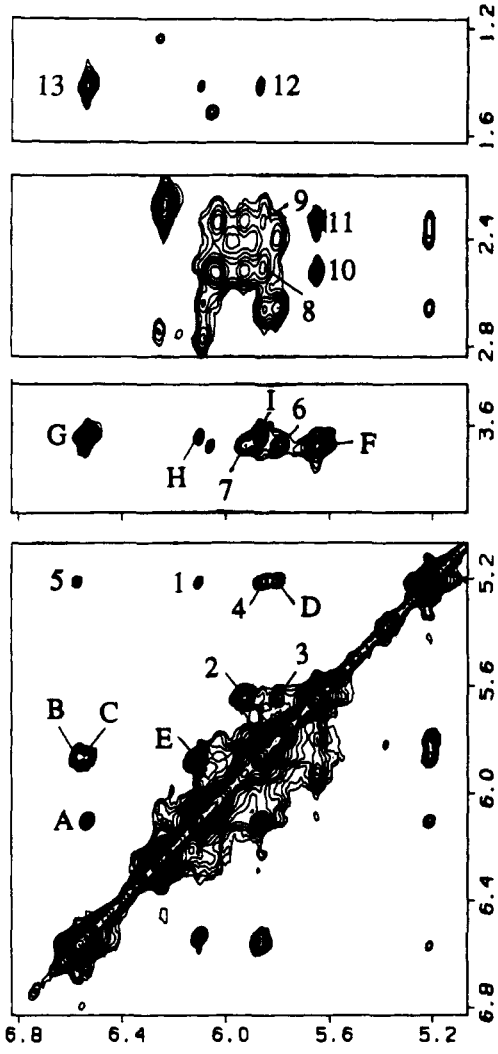

FIGURE 5: Expanded NOESY contour plots (mixing time, 75 ms) of the d(A-A-T-[ST]G-C-A-T-T) adduct duplex in D_2O buffer at 5 °C. Contour plot correlating the H1′ region (5.1–6.8 ppm) to various other regions (5.1–6.8 ppm; 3.5–3.9 ppm; 2.2–2.8 ppm; 1.2–1.6 ppm) in the spectrum. The intramolecular cross peaks A–I are assigned as follows: (A) ST(H3a)–ST(H2); (B) ST(H11)–ST(H9); (C) ST(H3a)–ST(H1); (D) G4(H1′)–C5(H5); (E) ST(H2)–ST(H1); (F) ST(H5)–ST(OCH_3-6); (G) ST(H3a)–ST(H12c); (H) ST(H2)–ST(H12c); (I) ST(H1)–ST(H12c). The intermolecular NOE cross peaks 1–13 are assigned as follows: (1) ST(H2)–C5(H5); (2) ST(H5)–T3(H1′); (3) ST(H5)–G4(H1′); (4) ST(H9)–C5(H5); (5) ST(H11)–C5(H5); (6) ST(OCH_3-6)–G4(H1′); (7) ST(OCH_3-6)–T3(H1′); (8) ST(H9)–C5(H2″); (9) ST(H9)–C5(H2′); (10) ST(H5)–T3(H2″); (11) ST(H5)–T3(H2′); (12) ST(H3a)–T3(CH_3); (13) ST(H1)–T3(CH_3).

OH-8 containing edge of the phenolic ring of sterigmatocystin is positioned in the minor groove. By contrast, both the ST(H10) and ST(H11) aromatic protons exhibit NOEs to the major groove C5(H5) protons (see peak 5, Figure 5, for the latter NOE), positioning the H10 and H11 edge of the phenolic ring of sterigmatocystin in the major groove. These intermolecular NOEs position the aromatic rings of sterigmatocystin between the T3·A6 and [ST]G4·C5 base pairs, which is consistent with intercalation of the aromatic chromophore into the duplex at the (T3-[ST]G4)·(C5-A6) step in the d(A1-A2-T3-[ST]G4-C5-A6-T7-T8) adduct duplex. The observed intermolecular NOEs in the adduct duplex are tabulated in Table IV.

We have also undertaken parallel studies on the self-complementary d(A-A-A-[ST]G-C-T-T-T] adduct duplex **6** where the central A3-[ST]G4-C5-T6 segment differs from the central T3-[ST]G4-C5-A6 segment in the adduct duplex discussed above. Such a comparative study helps to confidently assign cross peaks in regions of spectral overlap and provides an independent check of the structural conclusions. The intermolecular NOEs in the d(A-A-A-[ST]G-C-T-T-T) adduct duplex are listed in Table V and establish that the aromatic chromophore of sterigmatocystin intercalates between the [ST]-G4·C5 and A3·T6 base pairs. Only minor chemical shift

Table III: Chemical Shifts of the Sterigmatocystin Protons in the d(A-A-T-[ST]G-C-A-T-T) and d(A-A-A-[ST]G-C-T-T-T) Adduct Duplexes in Aqueous Buffer at 5 °C

	chemical shifts (ppm)		
proton	$\delta_{A\text{-}A\text{-}T\text{-}[ST]G\text{-}C\text{-}A\text{-}T\text{-}T}$	$\delta_{A\text{-}A\text{-}A\text{-}[ST]G\text{-}C\text{-}T\text{-}T\text{-}T}$	$\Delta\delta$
H2	6.09	6.08	0.01
H1	5.85	5.77	0.08
H12c	3.63	3.86	–0.23
H3a	6.52	6.57	–0.05
H5	5.63	5.51	0.12
OCH_3-6	3.66	3.61	0.05
OH-8[a]	11.06	11.87	–0.81
H9	5.84	5.86	–0.02
H10	7.13	7.13	0.00
H11	6.55	6.57	–0.02

[a] Chemical shift in H_2O solution.

Table IV: Intermolecular NOEs between Sterigmatocystin and Nucleic Acid Protons in the d(A-A-T-[ST]G-C-A-T-T) Adduct Duplex

ST protons	nucleic acid protons
H1	T3(CH_3)[a]
H2	C5(H5),[a] [ST]G4(H8)
H12c	T3(CH_3), T3(H6)
H3a	T3(CH_3), T3(H6), [ST]G4(H8), T3(H2′),[a] T3(H2″)[a]
H5	T3(H1′), T3(H2′), T3(H2″), [ST]G4(H8),[a] [ST]G4(H1′)
OCH_3-6	[ST]G4(H1′), A6(H2), T3(H1′)
OH-8	A6(H8), C5(H1′), C5(H2′),[a] C5(H2″),[a] A6(H1′), [ST]G4(NH_2-2b), [ST]G4(NH_2-2e)
H9	C5(H1′), C5(H2′), C5(H2″), C5(H5), C5(H6)[a]
H10	C5(H5), C5(H2′),[a] C5(H2″)[a]
H11	C5(H5)

[a] These are weak NOEs.

Table V: Intermolecular NOEs between Sterigmatocystin and Nucleic Acid Protons in the d(A-A-A-[ST]G-C-T-T-T) Adduct Duplex

ST protons	nucleic acid protons
H1	
H2	C5(H5),[a] [ST]G4(H8)
H12c	A3(H8)
H3a	A3(H8), [ST]G4(H8), A3(H2'),[a] A3(H2'')[a]
H5	A3(H1'), A3(H2'), A3(H2''), [ST]G4(H8),[a] [ST]G4(H1'), A3(H8)[a]
OCH_3-6	[ST]G4(H1'), A3(H2), A3(H1'), A3(H8),[a] A3(H2'),[a] A3(H2''),[a] [ST]G4(H2'),[a] [ST]G4(H2''),[a] [ST]G4(H3')
OH-8	T6(CH_3), C5(H1'), C5(H2'), C5(H2''), T6(H1'), [ST]G4(NH_2-2b),[ST]G4(NH_2-2e), A3(H2)
H9	C5(H1'), C5(H2'), C5(H2''), C5(H5), C5(H6), T6(H6), T6(CH_3)
H10	C5(H5), C5(H2'),[a] C5(H2''),[a] C5(H6),[a] T6(CH_3)
H11	C5(H5), T6(CH_3)[a]

[a] These are weak NOEs.

Table VI: Chemical Shifts of the [ST]G4·C5 Base Pair Protons in the d(A-A-T-[ST]G-C-A-T-T) and d(A-A-A-[ST]G-C-T-T-T) Adduct Duplexes in Aqueous Buffer at 5 °C

proton	chemical shifts (ppm) $\delta_{A\text{-}A\text{-}T\text{-}[ST]G\text{-}C\text{-}A\text{-}T\text{-}T}$	$\delta_{A\text{-}A\text{-}A\text{-}[ST]G\text{-}C\text{-}T\text{-}T\text{-}T}$	$\Delta\delta$
[ST]G4(H8)	9.58	9.51	0.07
[ST]G4(H1')	5.78	5.83	–0.05
[ST]G4(H2')	2.39	2.39	0.00
[ST]G4(H2'')	2.66	2.70	–0.04
[ST]G4(H3')	4.79	4.78	0.01
[ST]G4(H4')	4.37	4.40	–0.03
[ST]G4(NH-1)	12.89	12.86	0.03
[ST]G4(NH_2-2b)	8.83	8.81	0.02
[ST]G4(NH_2-2e)	6.71	6.72	–0.01
C5(H6)	7.47	7.47	0.00
C5(H5)	5.20	5.24	–0.04
C5(H1')	6.01	6.09	–0.08
C5(H2')	2.34	2.33	0.01
C5(H2'')	2.53	2.50	0.03
C5(H3')	4.85	4.90	–0.05
C5(H4')	4.18	4.16	0.02
C5(NH_2-4b)	7.12	7.16	–0.04
C5(NH_2-4e)	6.71	6.72	–0.01

differences are observed for the [ST]G4·C5 base pair protons between the d(A-A-T-[ST]G-C-A-T-T) and d(A-A-A-[ST]G-C-T-T-T) duplexes (Table VI) establishing similar stacking overlaps between the intercalated chromophore of sterigmatocysin and the common [ST]G4·C5 base pair in the two adduct duplexes. The sterigmatocystin protons also exhibit similar chemical shifts in the two adduct duplexes (Table III) with the exception of the OH-8 proton, which is shifted downfield by 0.8 ppm in the d(A-A-A-[ST]G-C-T-T-T) adduct duplex compared to the d(A-A-T-[ST]G-C-A-T-T) adduct duplex.

Experimental Distance Bounds. Our protocol for measuring the interproton distances bounds in the d(A-A-T-[ST]G-C-A-T-T) adduct duplex based on 50- and 75-ms mixing time NOESY data sets in D_2O and a 150-ms mixing time NOESY data set in H_2O is outlined under Materials and Methods. A set of distance bounds corresponding to the 28 intermolecular distance constraints in the adduct duplex are listed in Table VII. We did not estimate distance bounds for those cross peaks involved in spectral overlap in the NOESY spectra of the adduct duplex. These 28 intermolecular distance bounds along with 90 constraints between nucleic acid protons and eight constraints between sterigmatocystin protons in the adduct duplex were incorporated in the molecular dynamics simulation and correspond to a total of 126 constraints for one

Table VII: Comparison of Distance Bounds between Sterigmatocystin and Nucleic Acid Protons with Corresponding Distances in the NMR–Molecular Dynamics Refined Structure of the d(A-A-T-[ST]G-C-A-T-T) Adduct Duplex

intermolecular proton pairs	distance bounds (Å)	actual distance (Å)
ST(H1)–T3(CH_3)	3.5–5.3	5.4
ST(H2)–[ST]G4(H8)	2.5–4.5	3.3
ST(H2)–C5(H5)	3.6–5.4	5.4
ST(H3a)–T3(H6)	2.8–4.2	3.4
ST(H3a)–[ST]G4(H8)	3.5–5.5	4.3
ST(H3a)–T3(CH_3)	2.2–3.4	3.3
ST(H3a)–T3(H2')	3.5–5.5	3.9
ST(H3a)–T3(H2'')	3.5–5.5	4.3
ST(H12c)–T3(H6)	3.5–5.5	4.2
ST(H12c)–T3(CH_3)	2.2–3.4	3.2
ST(H5)–[ST]G4(H1')	2.8–4.2	3.7
ST(H5)–T3(H1')	2.5–3.7	3.3
ST(H5)–T3(H2')	2.5–4.3	4.2
ST(H5)–T3(H2'')	2.3–4.1	2.6
ST(H5)–A6(H2)	3.5–5.5	4.7
ST(OCH_3-6)–[ST]G4(H1')	2.3–3.5	3.6
ST(OCH_3-6)–T3(H1')	2.7–4.1	4.3
ST(OCH_3-6)–A6(H2)	2.4–3.8	3.6
ST(OH-8)–[ST]G4(NH_2-2b)	3.0–5.0	3.2
ST(OH-8)–[ST]G4(NH_2-2e)	3.0–5.0	3.2
ST(OH-8)–A6(H1')	3.5–5.5	3.8
ST(OH-8)–C5(H1')	2.5–4.5	3.6
ST(OH-8)–C5(H2')	3.5–5.5	4.2
ST(OH-8)–C5(H2'')	3.0–5.0	3.0
ST(H9)–C5(H2')	2.4–4.2	2.7
ST(H9)–C5(H6)	2.8–4.2	4.6
ST(H9)–C5(H5)	2.9–4.3	4.5
ST(H10)–C5(H5)	2.5–3.9	3.2

symmetrical half of the d(A-A-T-[ST]G-C-A-T-T) adduct duplex.

Starting Models for Structure Refinement. The d(A-A-T-G-C-A-T-T) duplex was generated from the coordinates of a standard B-form structure. The C^2 position of sterigmatocystin was covalently linked to the N^7 position of G4 with the distance between them fixed at 1.5 Å. The dihedral angles in the bisdihydrofuran ring of sterigmatocystin were obtained from crystallographic data on related systems (van Soest & Peerdeman, 1970). Two different initial structures of the adduct duplex were generated for the molecular dynamics computations as a test for the covergence characteristics of the final refined structures. One initial structure of the adduct was generated by inserting the aromatic ring of the covalently linked sterigmatocystin at the (T3-[ST]G4)·(C5-A6) step without separation of the [ST]G4·C5 and T3·A6 base pairs. This starting structure called Init A is shown in Figure S1A (Supplementary Material). A second starting structure of the adduct was generated by cleaving the duplex at the T3–[ST]G4 and C5–A6 steps and increasing the separation between the [ST]G4·C5 and T3·A6 base pairs by a factor of 2. The aromatic ring of the covalently linked sterigmatocystin was inserted between these base pairs. This starting structure called Init B is shown in Figure S1B (Supplementary Material). Removal of bad steric contacts in the Init A starting structure and ligation of the backbone atoms on each strand at the intercalation site in the Init B starting structure was achieved during subsequent minimization.

Structure Refinement. The Init A and Init B structures served as starting models for structure refinement using molecular dynamics computations with NMR-based distance bounds as input constraints using previously published protocols (Zhang & Patel, 1990, 1991; Liu et al., 1991). The final structures of the d(A2-T3-[ST]G4-C5-A6-T7) segment of the adduct duplex which were refined from the two starting

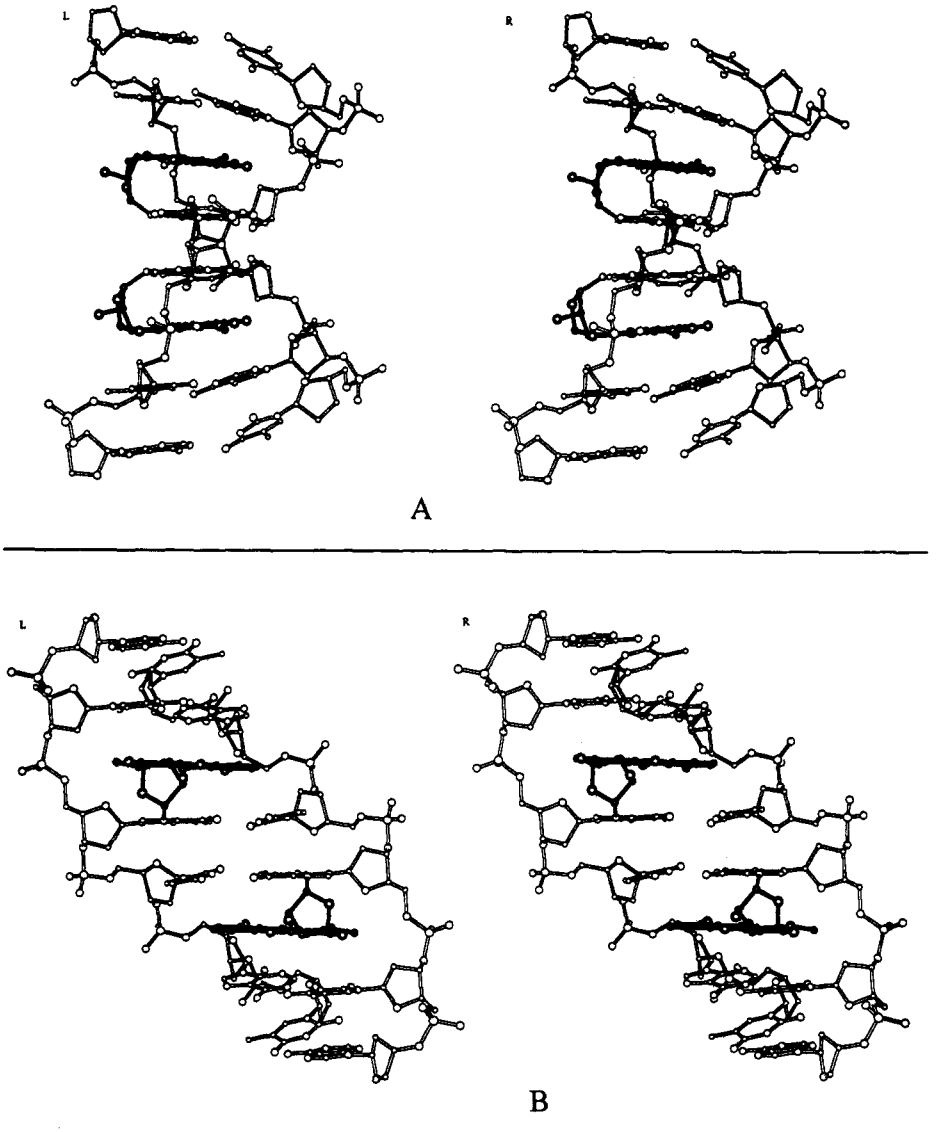

FIGURE 6: Stereoviews of one final structure of the d(A-A-T-[ST]G-C-A-T-T) adduct duplex. The terminal A·T base pairs at either end are deleted. (A) Side view with the major groove on the left and the minor groove on the right. (B) View looking into the major groove.

structures are superpositioned on the basis of a best fit for all heavy atoms in Figure S2 (Supplementary Material) and exhibit a root-mean-square deviation of 0.9 Å.

One of these final structures for the d(A-A-T-[ST]G-C-A-T-T) adduct duplex (lacking the terminal A1·T8 base pairs at either end of the helix) is plotted in stereo with the emphasis on two different views in Figure 6. The intermolecular interproton distances measured for this structure of the adduct duplex show good agreement with the experimental distance bounds used in the molecular dynamics calculation (Table VII).

Structural Features of the NMR–MD Refined Adduct Duplex. Several features of the d(A-A-T-[ST]G-C-T-A-A) adduct duplex stand out and provide new insights into how a mutagen can simultaneously covalently bind to and intercalate between base pairs of a right-handed double helix. In the present study, the covalent linkage occurs at the N^7 position of guanine in the major groove and intercalation of the attached aromatic component is facilitated by reversal in direction due to the fused ring geometry of the bisdihydrofuran component of sterigmatocystin. The long axis of the sterigmatocysin aromatic chromophore is colinear with the long axis of the base pairs at the intercalation site (Figure 7). The intercalation site is 5′ to the modified guanine permitting modification at adjacent guanines on partner strands in (G-C)·(G-C) steps.

Covalent Linkage Site. The geometry at the covalent linkage site connecting the C^2 of sterigmatocystin and the N^7 of [ST]G4 impacts on the structure of the adduct duplex. The C^2 atom is out of the plane of the purine ring of [ST]G4 in the refined structure of the adduct duplex (Figures 6 and 7). This reflects the formation of a tetrahedral nitrogen at N^7 of the purine base of [ST]G4 following adduct formation. The dihedral angle at the C^8-N^7-ST(C^2)-ST(C^1) covalent linkage bond was 123° in the refined structure of the adduct duplex.

Sterigmatocystin Conformation in Adduct Duplex. The mean plane of the tetrahydrofuran ring A of sterigmatocystin is parallel to the helix axis and spans half the intercalation site generated between the T3·A6 and [ST]G4·C5 base pairs. The H1 and H2 protons of ring A are on opposite sides of the puckered tetrahydrofuran ring with a dihedral angle between them of 77°.

The remaining ring systems B, C, D, and E of sterigmatocystin form a planar aromatic component that intercalates between the bases on both strands in the adduct duplex. The long edge of this planar chromophore containing the OH-8 and OCH_3-6 groups is positioned in the minor groove while the long edge containing the H10 and H11 protons is positioned in the major groove. In essence, tetrahydrofuran ring A acts as a fixed bridge or staple between the covalent linkage site and the aromatic chromophore and positions the latter for

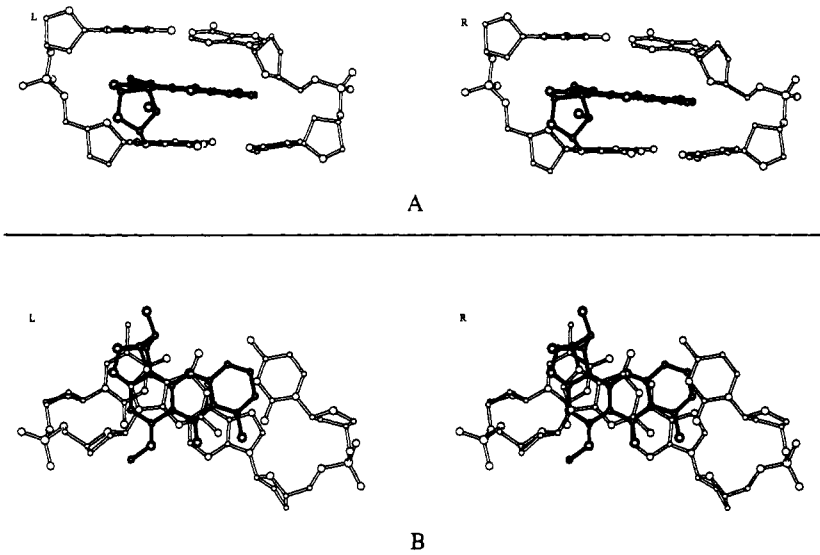

FIGURE 7: Stereoviews of the (T3-[ST]G4)·(C5-A6) intercalation site in the d(A-A-T-[ST]G-C-A-T-T) adduct duplex. (A) View looking into the major groove. This view emphasizes the covalent linkage between G4(N^7) and ST(C^2). (B) View looking down the helix axis. This view emphasizes the overlap geometry of the sterigmatocystin chromophore with the flanking T3·A6 and [ST]G4·C5 base pairs.

Table VIII: Selective Helical Parameters[a] in the NMR–MD Refined Structure of d(A-A-T-[ST]G-C-A-T-T) Adduct Duplex

base	χ^b	P[c] (pucker)
A2	−114	186 (C3′-exo)
T3	−121	144 (C1′-exo)
[ST]G4	−131	146 (C2′-endo)
C5	−133	115 (C1′-exo)
A6	−119	143 (C1′-exo)
T7	−130	150 (C2′-endo)

[a] Derived using the CURVE program. [b] Glycosidic torsion angle. [c] Sugar pucker pseudorotation value.

Table IX: Twist Angles between Base Pairs[a] in the NMR–MD Refined Structure of d(A-A-T-[ST]G-C-A-T-T) Adduct Duplex

base pairs	twist angle
T3·A6 and A2·T7	30°
[ST]G4·C5 and T3·A6	29°
[ST]G4·C5 and [ST]G4·C5	38°

[a] Derived using the CURVE program.

intercalation 5′ to the adducted guanine.

The OH-8 proton of ST[G4] can form an intermolecular hydrogen bond with the O4′ sugar ring oxygen of A6 on the partner strand (H···O length is 2.6 Å; O–H···O angle is 103°) and potentially anchors the stacking alignment at the intercalation site.

DNA Conformation in Adduct Duplex. Qualitative analysis of the NOE cross peak patterns and intensities on the d(A-A-T-[ST]G-C-A-T-T) adduct duplex in H_2O and D_2O establishes that the helix is right-handed with nonterminal A·T and [ST]G·C base pairs adopting Watson–Crick alignment, that the glycosidic torsion angles are in the anti range, and that the sugar puckers are in the C2′-endo range. The glycosidic torsion angles and the sugar pucker pseudorotation angles for the (A2-T3-[ST]G4-C5-A6-T7) segment of the refined structure of the adduct duplex are listed in Table VIII.

The helix twist angle between the base pairs varies with the particular step in the refined structure of the d(A1-A2-T3-[ST]G4-C5-A6-T7-T8) adduct duplex (Table IX). The helix twist angle of 29° between the [ST]G4·C5 and T3·A6 base pairs represents an unwinding of 7° at the intercalation site. There is also an unwinding of 6° between the T3·A6 and A2·T7 base pairs one removed from the intercalation site and directed toward the ends of the helix (Table IX). By contrast, the central [ST]G4–C5 step is sandwiched between the two symmetrical intercalation sites and is slightly overwound by 2° in the adduct duplex. This amounts to a net unwinding of 24° for the (A2-T3-[ST]G4-C5-A6-T7)·(A2-T3-[ST]G4-C5-A6-T7) segment in the adduct duplex.

Intercalation Site Geometry and Intermolecular Stacking Interactions. The sterigmatocystin aromatic chromophore spans the intercalation site so that the T3·A6 and [ST]G4·C5 base pairs are separated by 6.8 Å and are essentially parallel to each other (Figure 7A). The majority of the overlap between the sterigmatocystin chromophore and flanking base pairs is observed with the T3–[ST]G4 step while minimal overlap is observed with the C5–A6 step (Figure 7B). Specifically, sterigmatocystin ring B overlaps with T3 in one direction while sterigmatocystin rings C and D overlap with [ST]G4 in the other direction. By contrast, sterigmatocystin ring E does not overlap with either the C5 or A6 bases on the partner strand (Figure 7B).

DISCUSSION

Reaction of Sterigmatocystin-1,2-epoxide with DNA. We have followed the procedure of Baertschi et al. (1988) in synthesizing the sterigmatocystin-1,2-epoxide following treatment of sterigmatocystin with dimethyldioxyrane. Sterigmatocystin-1,2-epoxide is sparingly soluble in aqueous buffer. Hence, the reaction was carried out in a two-phase system with epoxide present in methylene chloride and the DNA in aqueous buffer. The reaction was extremely slow and took 7–10 days to achieve 50% completion. During the course of the reaction the hydrolysis of the sterigmatocystin epoxide was minimal. This is in sharp contrast to aflatoxin B_1 epoxide, whose half-life in aqueous medium was on the order of seconds (Baertschi et al., 1988) but is known to react rapidly with DNA. It is likely that the added stability of sterimatocystin epoxide as well as its slow reaction with DNA in water/methylene chloride solvent system was due to preferential partioning in the organic layer and rapid crystallization of the epoxide.

The reaction of sterigmatocystin epoxide was carried out with d(A-A-T-G-C-A-T-T) and d(A-A-A-G-C-T-T-T) du-

plexes. Both self-complementary sequences form duplexes with 2-fold symmetry and are capable of forming adducts with the N^7 of guanine on both strands. Two squences were chosen so as to check the internal consistency of the structure of the adduct. Our results clearly establish that the reaction of sterigmatocystin-1,2-epoxide with both DNA oligomers exhibits a stoichiometry of two modified guanines per duplex. This is possible only if the epoxide were to orient toward the 5′ side of guanine in the duplex since orientation toward the 3′ side would result in steric clashes precluding the modification of the second guanine (Gopalakrishnan et al., 1990).

Instability of the Adduct. The N^7-guanine adducts of compounds like aflatoxin B_1 and methylhalides have been known to deshield the H8 proton of guanine because of the presence of the positive charge in the purine ring. In the case of aflatoxin B_1–N^7-guanine adduct at the duplex level, the H8 proton was observed at 9.78 ppm (Gopalakrishnan et al., 1990). We also observe a downfield-shifted [ST]G4(H8) proton in the sterigmatocystin adduct at the duplex level. The N^7-guanine adducts of aflatoxin B_1 have been known to be very labile both in vitro and in vivo (Busby & Wogan, 1984) and undergo three types of decomposition. (i) The carcinogen can be cleaved off, leaving behind intact DNA. (ii) The adduct depurinates, creating an apurinic site. (iii) The guanine ring opens to form a formamidopyrimidine adduct (FAPY adduct). Previous experience with oligonucleotide adducts of aflatoxin B_1 (Gopalakrishnan et al., 1989, 1990) as well as the current studies on adducts of sterigmatocystin suggest that the half-life of the adduct is of the order of few hours at room temperature. The stability can be enhanced by lowering the temperature to 5 °C, conditions under which the half-life is around 7 days. The purified adducts can be stored in the freezer at −22 °C for longer periods of time.

Spectral Markers. The protons distributed throughout the sterigmatocystin ring system have been assigned in the d(A-A-T-[ST]G-C-A-T-T) adduct duplex (Table III). This information together with the corresponding intermolecular NOEs involving protons on sterigmatocystin rings A, B, C and E (Table IV) define the complementarity of the fit between the mutagen and the DNA.

The base and sugar DNA protons have also been assigned in the d(A-A-T-[ST]G-C-A-T-T) adduct duplex (Tables I and II). The guanine amino protons are generally broad in DNA oligomer duplexes because of intermediate rotation rates about the C^2–NH_2 bond of guanine (Patel, 1976). However, we observe separate hydrogen-bonded (8.83 ppm) and exposed (6.71 ppm) amino protons for [ST]G4 in the adduct duplex. These exchangeable amino protons provide markers in the minor groove at the adduct site, and intermolecular NOEs involving these protons (Table IV) help to define complementary interactions between sterigmatocystin and the DNA in the minor groove.

The H8 proton of [ST]G4 exhibits an unusual chemical shift of 9.58 ppm for the sterigmatocystin adduct duplex (Figure 1A) similar to what was reported previously for the aflatoxin adduct duplex (Gopalakrishnan et al., 1989, 1990). Its downfield shift and its lability to exchange reflects protonation of the adjacent N^7 position on adduct formation. In the present study, several critical intermolecular NOEs were observed involving this downfield-shifted proton (Table IV) and help to position the sterigmatocystin adduct on the DNA.

Similarly, the sterigmatocystin OH-8 proton at 11.06 ppm can be detected as a narrow resonance and exhibits a large number of intermolecular NOEs (Table IV) that define the complementarity of the fit in the minor groove. Clearly, the use of intermolecular NOEs involving exchangeable protons in the present study of the sterigmatocystin–DNA adduct duplex have provided the additional constraints necessary to define the solution structure of the d(A-A-T-[ST]G-C-A-T-T) adduct duplex.

Base and Orientation Specificity of Adduct Formation. The pioneering studies on aflatoxin adducts with the self-complementary d(A-T-G-C-A-T) and d(A-T-C-G-A-T) duplexes established unequivocally that aflatoxin binds to the N^7 of guanine with its aromatic chromophore intercalated above the 5′ face of the modified guanine (Gopalakrishnan et al., 1989, 1990). The same base and orientation specificity of adduct formation is also observed in the present study of the sterigmatocystin adducts with the self-complementary d(A-A-T-G-C-A-T-T) and d(A-A-A-G-C-T-T-T) duplexes. Clearly, the four asymmetric carbon centers on fused rings A/B which are common to both aflatoxin and sterigmatocystin adducts (see **4**) must define the orientational specificity of the binding.

There does not appear to be any preference for a particular base either to the 5′ or the 3′ side of the modified guanine with respect to adduct formation. This is not surprising since the stacking interactions associated with intercalation are likely to be minimally dependent on the type of base pair 5′ to the modified guanine.

Covalent Linkage Site. An important feature of the structure of the sterigmatocystin–DNA adduct is the geometry at the covalent linkage that connects the N^7 of guanine with the C^2 of sterigmatocystin. Theoretical studies have suggested that the C^2 atom be out of the plane of the purine base as a consequence of sp^3 hybridization at the N^7 position on adduct formation (Bonnett & Taylor, 1989). Such a geometry has also been observed for N^7-guanine adducts of cobalt complexes (Liaw et al., 1990). The solution structure of the sterigmatocystin–DNA adduct duplex clearly shows the C^2 atom of sterigmatocystin to be out of the plane of the guanine of [ST]-G4 (Figures 6 and 7).

The tetrahydrofuran ring A and the dihydrofuran ring B of sterigmatocystin exhibit puckered geometries characteristic of five-membered rings in the structure of the adduct duplex. Sterigmatocystin ring A plays a pivotal role since it spans the distance between the covalent site and the intercalating chromophore and aligns the chromophore parallel to the modified guanine plane. The L-shaped structure of sterigmatocystin is thus ideally suited for covalent bond formation and intercalation, and it remains to be established whether intercalative binding precedes covalent adduct formation. It is also interesting that aflatoxin and sterigmatocystin form adducts with the N^7 position of guanine but not with the N^7 position of adenine even though both these positions are potential target sites for adduct formation.

Intercalation Site. The early NMR studies on aflatoxin–DNA adducts established that not only does the mycotoxin covalently attach to the N^7 of guanine but, in addition, it intercalates along the 5′ face of the modified base (Gopalakrishnan et al., 1989, 1990). The present NMR studies on the sterigmatocystin–DNA adduct strongly support this conclusion and extend these observations to the quantitative structural characterization of the adduct duplex which defines details of the intercalation site and the nature of the overlaps stabilizing the adduct duplex.

The absence of characteristic NOEs between adjacent residues at the T3–[ST]G4 and C5–A6 steps in the d(A-A-T-[ST]G-C-A-T-T) adduct duplexes establishes that the

intercalation site is between the T3·A6 and [ST]G4·C5 base pairs. The observed intermolecular NOEs are consistent with the long axis of the sterigmatocystin chromophore being colinear with the long axis of the T3·A6 and [ST]G4·C5 base pairs at the intercalation site. Such an alignment is similar to overlaps observed in actinomycin intercalation complexes (Liu et al., 1991) and luzopeptin bisintercalation complexes (Zhang & Patel, 1991) but different from the nogalamycin intercalation complexes (Zhang & Patel, 1990; Williams et al., 1990; Liaw et al., 1989) where the long axis of the intercalating chromophore was orthogonal to the long axis of the flanking base pairs.

The planar chromophore of sterigmatocystin spans the entire intercalation cavity so that the flanking base pairs are approximately parallel to each other (Figure 7A) in contrast to the buckling of the base pairs observed in the nogalamycin intercalation complex (Zhang & Patel, 1990). The polar edge of the sterigmatocystin chromophore containing the OH-8, carbonyl-7, and OCH_3-6 groups is directed toward the minor groove, while the predominately nonpolar edge faces the major groove.

There are no unusual features associated with the intercalation site in that the helix is unwound, the base pairs are Watson–Crick, and both the glycosidic torsion angles and sugar puckers are in the B-DNA family of conformations. Adduct formation results in a widening of the minor groove by 1.2 Å as reflected in the shortest phosphorus–phosphorus separation across this groove in the d(A-A-T-[ST]G-C-A-T-T) adduct duplex.

Charge Delocalization in the Imidazole Ring of the Modified Guanine. Our structure establishes that intercalation of the sterigmatocystin chromophore forces the C^2–N^7 covalent linkage out of planarity with the rest of the modified guanine ring. This results in a tetrahedral geometry at the N^7 of the modified guanine which in turn suggests that the positive charge in the imidazole ring is delocalized over the C^8 and N^9 positions. This charge delocalization is reflected in the HPLC-detected decomposition products of the d(A-A-T-[ST]G-C-A-T-T) adduct duplex as a function of time at neutral and basic pH. Thus, at neutral pH, we detect primarily cleavage at the glycosidic bond resulting in formation of an apurinic site which is consistent with charge delocalization to N^9 of the modified guanine ring. By contrast, at basic pH, FAPY adduct formation predominates, corresponding to opening of the imidazole ring through solvent attack at the C^8 position, and reflects charge delocalization to C^8 of the modified guanine ring.

These results may be compared with the decomposition adducts of guanine N^7 modification by simple alkylating agents lacking potential intercalating chromophores (Muller & Eisenberg, 1985; Humphreys & Guengerich, 1991). It was established that FAPY adduct formation was greatly facilitated in aflatoxin-modified guanine-N^7 adducts in contrast to ethylene dibromide-modified guanine-N^7 adducts (Humphreys & Guengerich, 1991). This may reflect the greater charge delocalization at the guanine C^8 position resulting from a tetrahedral geometry at the N^7 position in the aflatoxin-modified guanine adduct.

Comparison with Molecular Modeling Studies. Our results can be compared with a molecular modeling study that investigated the range of potential structures available to aflatoxin when covalently linked to the N^7 of guanine at the DNA oligomer level (Loechler et al., 1988). These workers presented both external binding and intercalation models for the aflatoxin adduct. The preferred model had aflatoxin positioned in the major groove with its long axis perpendicular to the helix axis. We find no evidence in our experimental data to support this model. The less preferred model had the covalently linked aflatoxin intercalated into the duplex on the 5′ side of the adducted guanine. This result anticipated the conclusions from the NMR investigations (Gopalakrishnan et al., 1990; this study) with the important distinction that the tetrahedral geometry at N^7 was not considered in the modeling study.

Comparison of Aflatoxin and Sterigmatocystin Adducts. The NMR studies on the aflatoxin–DNA adduct (Gopalakrishnan et al., 1989, 1990) and the NMR–molecular dynamics studies on the sterigmatocystin–DNA adduct reported in this study establish that both mutagens bind to the N^7 of guanine and intercalate over the 5′ face of the adducted guanine. Since rings A, B, and C are common to both aflatoxin and sterigmatocystin, the only differences between the two adducts must originate in the different overlaps between ring E and flanking base pairs. There is minimal overlap between sterigmatocystin ring E and the bases on the unmodified strand at the intercalation site (Figure 7B). By contrast, replacing ring E of sterigmatocystin **1** by ring E of aflatoxin **2** should result in greater stacking in the same sequence context. The hydrogen-bonding donor/acceptor functionalities on rings D and E occupy different spatial positions in aflatoxin and sterigmatocystin so that different intermolecular hydrogen-bonding interactions are also feasible.

ACKNOWLEDGMENT

Dr. Gopalakrishnan thanks Drs. T. M. Harris and M. P. Stone for introducing him to the food mycotoxin field and for continued encouragement and discussion during the course of this research. The NMR spectrometers were purchased with funds donated by the Robert Woods Johnson Jr. Trust and Matheson Trust toward setting up the NMR Center in the Basic Medical Sciences at Columbia University.

SUPPLEMENTARY MATERIAL AVAILABLE

Figure S1 showing stereoviews of Init A and Init B, the two starting structures in the molecular dynamics simulation of the d(A-A-T-[ST]G-C-A-T-T) adduct duplex, and Figure S2 showing stereoviews of the two superimposed final structures of the d(A-A-T-[ST]G-C-A-T-T) adduct duplex (3 pages). Ordering information is given on any current masthead page.

REFERENCES

Adamson, R. H. (1989) *Cancer Detect. Prev. 14*, 215–219.
Baertschi, S. W., Raney, K. D., Stone, M. P., & Harris, T. M. (1988) *J. Am. Chem. Soc. 110*, 7929–7931.
Baertschi, S. W., Raney, K. D., Shimada, T., Harris, T. M., & Guengerich, F. P. (1989) *Chem. Res. Toxicol. 2*, 114–122.
Bhatnagar, D., Cleveland, T. E., & Lillehoj, E. B. (1989) *Mycopathologia 107*, 75–83.
Bhatnagar, D., Cleveland, T. E., & Kingston, D. G. (1991) *Biochemistry 30*, 4343-4350.
Bonnett, M., & Taylor, E. R. (1989) *J. Biomol. Struct. Dyn. 7*, 127–149.
Bressac, B., Kew, M., Wands, J., & Ozturk, M. (1991) *Nature 350*, 429–431.
Busby, W. F., Jr., & Wogan, G. N. (1984) in *Chemical Carcinogens* (Searle, C., Ed.) 2nd ed., pp 945–1136, ACS monograph series 182, American Chemical Society, Washington, D.C.
Croy, R. G., Essigmann, J. M., Reinhold, V. N., & Wogan, G. N. (1978) *Proc. Natl. Acad. Sci. U.S.A. 75*, 1745–1749.

Dickens, F., Jones, H. E. H., & Waynforth, H. B. (1966) *Br. J. Cancer 20*, 134–144.
Dutton, M. E. (1988) *Microbiol. Rev. 52*, 274–295.
Essigmann, J. M., Croy, R. G., Nadzan, A. M., Busby, W. F., Reinhold, V. N., Buchi, G., & Wogan, G. N. (1977) *Proc. Natl. Acad. Sci. U.S.A. 74*, 1870–1874.
Essigmann, J. M., Barker, L. J., Fowler, K. W., Francisco, M. A., Reinhold, V. N., & Wogan, G. N. (1979) *Proc. Natl. Acad. Sci. U.S.A. 76*, 179–183.
Gopalakrishnan, S., Stone, M. P., & Harris, T. M. (1989) *J. Am. Chem. Soc. 111*, 7232–7239.
Gopalakrishnan, S., Harris, T. M., Stone, M. P. (1990) *Biochemistry 29*, 10438–10448.
Harris, C. C. (1991) *Cancer Res. (Suppl.) 51*, 5023s–5044s.
Holzapfel, C. W., Purchase, I. F. H., Steyn, P. S., & Gouws, L. (1966) *S. Afr. J. Nutr. 40*, 1100–1101.
Hsu, I. C., Metcalf, R. A., Sun, T., Welsh, J., Wang, N. J., & Harris, C. C. (1991) *Nature 350*, 427–428.
Humphreys, W. G., & Guengerich, F. P. (1991) *Chem. Res. Toxicol. 4*, 632–636.
Krivobok, S., Oliver, Ph., Marzin, D. R., Seigle-Murandi, F., & Steiman, R. (1987) *Mutagenesis 2*, 433–439.
Liaw, Y.-C., Gao, Y. G., Robinson, H., van der Marel, G. A., van Boom, J. H., & Wang, A. H. (1989) *Biochemistry 28*, 9913–9918.
Liaw, Y.-C., Gao, Y.-C., Robinson, H., Sheldrick, G. M., Sliedregt, L. A., Van der Marel, G. A., van Boom, J. H., & Wang, A. H.-J. (1990) *FEBS Lett. 264*, 223–227.
Liu, X., Chen, H., & Patel, D. J. (1992) *J. Biomol. NMR 1*, 323–347.
Loechler, E. L., Teeter, M. M., & Whitlow, M. D. (1988) *J. Biomol. Struct. Dyn. 5*, 1237–1257.
Mori, H., Sugie, S., Yoshimi, N., Kuniyasu, T., Iwata, H., Kawai, K., & Hamasaki, T. (1988) *Carcinogenesis 9*, 1039–1042.
Muller, N., & Eisenbrand, G. (1985) *Chem.-Biol. Interact. 53*, 173–181.
Murray, R. W., & Jayaraman, R. (1985) *J. Org. Chem. 50*, 2847–2853.
Patel, D. J. (1976) *Biopolymers 15*, 553–558.
Plateau, P., & Gueron, M. (1982) *J. Am. Chem. Soc. 104*, 7310–7311.
Purchase, I. F. H., & Van der Watt, J. J. (1969) *Food Cosmet. Toxicol. 7*, 135–139.
Purchase, I. F. H., & Van der Watt, J. J. (1970) *Food Cosmet. Toxicol. 8*, 289–295.
Purchase, I. F. H., & Van der Watt, J. J. (1973) *Toxicol. Appl. Pharmacol. 26*, 274–281.
Sahasrabudhe, S. R., Sambamurti, K., & Humayun, M. Z. (1989) *Mol. Gen. Genet. 217*. 20–25.
Sahasrabudhe, S. R., Luo, X., & Humayun, M. Z. (1990) *Biochemistry 29*, 10899–10905.
Schroeder, H. W., & Kelton, W. H. (1975) *Appl. Microbiol. 30*, 589–591.
Sreemannarayana, O., Frohlich, A. A., & Marquardt, R. R. (1987) *Mycopathologia 97*, 51–59.
Stoloff, L. (1989) *Regul. Toxicol. Pharamacol. 10*, 272–283.
Van der Watt, J. J., & Purchase, I. F. H. (1970) *Br. J. Exp. Pathol. 51*, 183–190.
Van Soest, T. C., & Peerdeman, A. F. (1970) *Acta Crystallogr. B26*, 1956–1963.
Wang, D. S., Sun, H. L., Xiao, F. Y., Ji, X. H., Liang, Y.-X., & Han, F. G. (1991) *IARC Sci. Publ. 105*, 424–426.
Williams, D. H., Egli, M., Gao, Q., Bash, P., van der Marel, G. A., van Boom, J. H., Rich, A., & Fredrick, C. (1990) *Proc. Natl. Acad. Scs. U.S.A. 87*, 2225–2229.
Wüthrich, K. (1986) *NMR of Proteins and Nucleic Acids*, Wiley, New York.
Xie, T. X. (1990) *Chung-hua Chung Liu Tsa Chih 12*, 21–23.
Yabe, K., Ando, Y., & Hamasaki, T. (1988) *Appl. Environ. Microbiol. 54*, 2101–2106.
Yabe, K., Ando, Y., Hashimoto, J., & Hamasaki, T. (1989) *Appl. Environ. Microbiol. 55*, 2172–2177.
Zhang, X., & Patel, D. J. (1990) *Biochemistry 29*, 9451–9466.
Zhang, X., & Patel, D. J. (1991) *Biochemistry 30*, 4026–4041.